Molecular dynamic simulations of the infrared dielectric response of silica structures

D. C. Anderson, J. Kieffer, and S. Klarsfeld

Citation: The Journal of Chemical Physics **98**, 8978 (1993); doi: 10.1063/1.464457
View online: http://dx.doi.org/10.1063/1.464457
View Table of Contents: http://scitation.aip.org/content/aip/journal/jcp/98/11?ver=pdfcov
Published by the AIP Publishing

Molecular dynamic simulations of the infrared dielectric response of silica structures

D. C. Anderson and J. Kieffer
Department of Materials Science and Engineering, University of Illinois, Urbana, Illinois 61801

S. Klarsfeld
Saint-Gobain Recherche, Aubervilliers, France 93303

(Received 21 December 1992; accepted 9 February 1993)

The molecular dynamic simulation technique was used to model the vibrational behavior of crystalline (α and β cristobalite) and amorphous silica structures. To this end a refined potential function was developed, which allows one to reproduce the correct structural geometries, the corresponding infrared spectra, and to observe a reversible phase transformation between α and β cristobalite. The complex dielectric constants in the infrared frequency range were calculated from the dipole moment time correlation functions. While idealized cristobalite exhibits the simplest spectrum with only two narrow bands, the increase of structural complexity and reduction of symmetry characteristic for the real cristobalites and amorphous silica, creates additional features in the infrared spectra. These structural changes predominantly affect the coordination of oxygen, and generate a broader spread in the normal modes characterizing the vibrations of this species. A unique method for the identification of atomic trajectories corresponding to the mechanisms responsible for individual absorption bands, which is based on the concept of Fourier transform filtering, is used for the assignment of absorption bands to atomic motions.

I. INTRODUCTION

The understanding of the structure and properties of materials has progressed considerably with the use of atomic scale numerical modeling techniques. This is particularly the case for substances with irregular structures, such as disordered crystals, liquids, and glasses. The purpose of this paper is to stress the fact that a reliable numerical model must be capable of accurately reproducing the structure as well as the vibrational properties of a simulated material. Given this capability, we show that the dynamic simulation technique can be used to identify signatures of structural disorder in the infrared spectra. Furthermore, we show how the analytical power of these numerical techniques can be exploited for the interpretation of experimental spectra.

Molecular dynamic and Monte Carlo simulations, where the minimum energy configurations are found iteratively following the constraints imposed by interatomic forces, proved to be particularly convenient for the modeling of atomic structures.[1,2] The pioneering theoretical work in this area, which took place in the sixties and early seventies, consisted in producing atomic coordinates which yielded structure factors matching those from diffraction experiments performed on the real materials.[3–5] Particle positions are determined by the location of the minima in the potential energy. The accurate reproduction of thermal properties, however, requires that the shape of the potential function near the minimum be represented with sufficient realism, since these properties involve oscillations of atoms about their equilibrium positions. Many of the early models for particle interaction fail in this respect. Consequently, the last decade has seen a vast effort towards the improvement of modeling of particle interactions.[6–9]

Especially for the modeling of glassy substances, it is necessary to use simulation ensembles that are as large as possible. (i) Since the simulation of bulk materials always involves periodic boundary conditions, only systems with more than several hundred atoms can provide a reasonable model for amorphous structures. (ii) In addition, elastic deformations usually propagate in a continuum. In small systems only those vibrational modes which are characterized by large wave vectors can exist. This precludes long wavelength modes from being accounted for in the numerically determined vibrational spectra, which can lead to a misrepresentation in the thermal and vibrational properties of the modeled systems.

The investigation of the nature of phonon spectra, which include acoustic and optical modes, is of great importance with respect to the design of materials for application in optics, optical fiber telecommunications, sensors, detectors, and optical storage media.[10] In particular, there is interest in isolating and analyzing the influence of structural disorder and defects on these spectra. To this end we undertook a systematic study of the infrared dielectric characteristics of a series of the structural modifications of silica. These include α and β cristobalite, ideal cristobalite, "disordered" cristobalite, as well as amorphous SiO_2. The comparison of diffraction patterns suggests that the structure of β quartz is closest to that of amorphous silica.[11] Nonetheless, for the interpretation of defect structures and vibrational spectra of amorphous silica,[12,13] it seemed appropriate to choose cristobalite as a reference, because of the similarities with regard to the electronic structure and chemical bonding in these two structures.[14,15]

Much of the quality of molecular dynamic simulations depends on the accuracy with which the atomic interac-

 0021-9606/93/116978-09$06.00

tions are modeled. The necessity to facilitate the simulation of large systems on the currently available computational resources, provides sufficient incentive for the improvement and the further development of semiempirical approaches to the modeling of atomic interactions. In the course of the simulation of an infrared absorption spectrum, the potential well is mapped over a finite energy range near its minimum. The accurate reproduction of experimental spectra of well characterized structures is used as an indicator for the meaningfulness of the potential functions used for the modeling of these structures, and serves as a guide for the development of effective models of interaction potentials.

II. COMPUTATIONAL PROCEDURE

A. Comparison of methodologies

Serious efforts towards the prediction of vibrational spectra by computational means, with the aim of assisting the interpretation of experimentally determined spectra, go back to the early 1960's. Initial attempts have utilized the approach of isolated "molecules," typically consisting of the basic structural unit, such as the SiO_4 tetrahedron, and the fundamental vibrational modes are derived based on the various possible deformations and symmetry operations. To overcome the effects of isolation, the molecules were "pinned" at strategic points,[16] or embedded in larger structural segments.[17] These early attempts, however, did not correctly account for the effects due to the propagation of elastic waves in three-dimensional continuous networks. It was not until the large-cluster calculations of Bell and Dean,[18] the central force network model of Sen and Thorpe,[19] or the Bethe lattice model of Laughlin and Joannopoulos[20] that artifacts attributable to a limited system size were significantly reduced.

There are, in principle, two computational procedures that permit one to attribute vibrational modes to the molecular structure: (i) the negative eigenvalue method and (ii) the time correlation method. The first one of these methods is based on the identification of a system of normal coordinates, along which occur the displacements of the vibrating particles. This normal coordinate system requires, in particular, the knowledge of the geometry of the structure. The equation of motion formulated for each particle at its equilibrium position yields the secular determinant

$$|\mathbf{D}_{ij}-\delta_{ij}\omega^2|=0, \tag{1}$$

where $\mathbf{D}_{ij}$ is the dynamical matrix, composed of the force constants attributed to each normal mode, δ_{ij} is the Dirac symbol, and ω the angular frequency. Assuming that the force constants are known, the secular determinant yields a polynomial in ω^2, whose roots are the eigenfrequencies observed in the vibrational spectrum of the molecule. Since the eigenfrequencies can be measured, sometimes the solution of the reverse problem is attempted, i.e., the determination of the force constant matrix. For this purpose, the system of equations, on which the secular equation is based, needs to be solved,

$$\mathbf{D}_{ij}\mathbf{u}_j=\omega^2\mathbf{u}_i, \tag{2}$$

where $\mathbf{u}$ is the displacement vector. In terms of the force constant matrix, this system of equations is underdetermined, i.e., there are more unknowns than equations. Additional information can be obtained by means of isotope substitutions. However, the problem is usually nontrivial.

In particular, it is necessary to have a fairly precise idea about the structure of the investigated substance. The more complex the structure, and the lower the symmetry, the more computationally intensive is the normal mode analysis and band assignment. Finally, in the case of highly defective, or amorphous structures, where the translational symmetry breaks down, it is questionable whether the normal mode analysis is an appropriate procedure.

With such complex structures in mind we used a different approach for the calculation of vibrational spectra. Using a technique such as molecular dynamic simulations, the trajectories in phase space can be recorded as a function of time. By constructing time correlation functions of the appropriate variables, it is possible to calculate the corresponding power spectra by means of taking the Fourier transform of these correlation functions. The strength of this method is that it provides static properties, i.e., the equilibrium structure and energetics, as well as dynamic properties, such as thermal characteristics and vibrational spectra, solely based on an appropriate model for particle interactions.

B. Molecular dynamic simulations

The molecular dynamic technique has become a fairly standard procedure for the investigation of the structure and properties of matter, and it is well documented in the literature.[1–3,21–24] Although there exist various enhancements to the basic algorithm, it essentially consists in the solution of a coupled system of differential equations, i.e., the equations of motion for each particle in the ensemble, using an explicit finite difference scheme. The accuracy of the procedure is determined by the size of the time step chosen. From the trajectory of the particles it is possible, by means of the formalisms of statistical thermodynamics, to extract virtually any physical property of the simulated system.

For example, we can calculate the infrared absorption spectra from the time development of the dipole moment, μ, of the simulation ensemble. We first record the time correlation function $\langle\dot{\mu}(0)\cdot\mu(t)\rangle$, whose Fourier transform then yields the frequency dependent complex dielectric constant,[25–27]

$$\epsilon(\omega)=1+4\pi\chi(\omega)=\int_{-\infty}^{\infty}\langle\dot{\mu}(0)\cdot\mu(t)\rangle e^{-i\omega t}dt$$

$$=\epsilon'(\omega)-i\epsilon''(\omega), \tag{3}$$

where ϵ' is the real and ϵ'' the imaginary part of the dielectric constant. The angular brackets in this case represent a time average, which means that a large number of

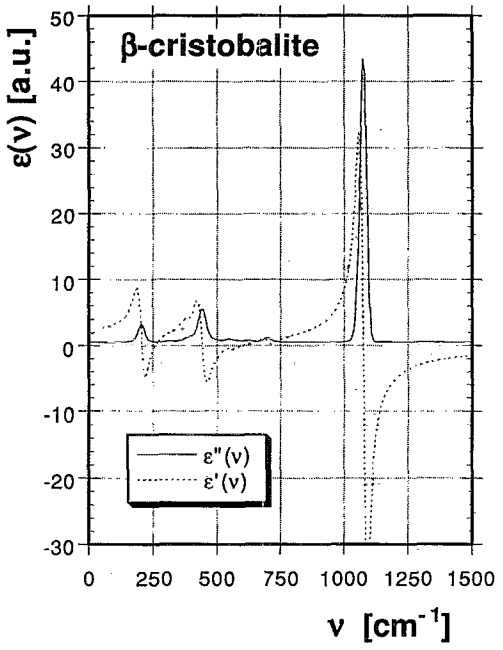

FIG. 1. Real (ϵ') and imaginary (ϵ'') part of the complex dielectric constant of β cristobalite, simulated at a temperature of 800 °C.

instants in the course of a simulation were chosen as time origins. The intensity of the absorbed radiation is then calculated according to

$$I(\omega)=\frac{\hbar\epsilon''}{4\pi^2(1-e^{-\hbar\omega/k_BT})}. \tag{4}$$

As an illustration the real and imaginary component of the complex dielectric constant is shown in Fig. 1 for a simulated β-cristobalite structure.

C. Particle interactions

The interaction model that we adapted for the present simulations is a potential function including two-body and three-body interactions. In a general form, the total potential energy of the system can be expressed as

$$U=\sum_{i<j}\phi_{ij}+\sum_{i<j<k}\phi_{ijk}, \tag{5}$$

where ϕ_{ij} acts between pairs of atomic particles and ϕ_{ijk} acts between triplets. In ceramic materials the fraction of ionic bonding is always relevant. Hence, the two-body interactions are

$$\phi_{ij}=\frac{z_iz_je^2}{4\pi\epsilon_0r_{ij}}+\frac{z_ie}{4\pi\epsilon_0r_{ij}^3}\boldsymbol{\mu}_j\cdot\mathbf{r}_{ij}+\frac{z_je}{4\pi\epsilon_0r_{ij}^3}\boldsymbol{\mu}_i\cdot\mathbf{r}_{ji}$$
$$+\frac{3}{4\pi\epsilon_0r_{ij}^5}(\boldsymbol{\mu}_j\cdot\mathbf{r}_{ij})(\boldsymbol{\mu}_i\cdot\mathbf{r}_{ij})-\boldsymbol{\mu}_i\cdot\boldsymbol{\mu}_j\frac{1}{4\pi\epsilon_0r_{ij}^3}$$
$$+A_{ij}\left(1+\frac{z_i}{n_i}+\frac{z_j}{n_j}\right)e^{(\sigma_i+\sigma_j-r_{ij})\rho_{ij}}, \tag{6}$$

where z_i are the valences of the ions, n_i are the number of electrons in the outer shell, r_{ij} is the distance between two particles, μ_i are electrostatic dipoles, A_{ij} and ρ_{ij} are empirical constants, e is the unit electron charge, and ϵ_0 the dielectric constant of the vacuum. In this equation the first three lines represent the charge–charge, charge-dipole, and dipole–dipole interactions respectively. The last line represents the repulsion between atoms resulting from the overlap of nonbonding orbitals. The chosen form is due to Born and Huggins-Mayer.[28] In the present study, we assumed dipoles to result from the polarization of the larger oxygen anions. The polarizabilities of the oxygen and silicon ions were assumed to 3.88×10^{-3} and 1.65×10^{-4} nm^3, respectively.[29] For each update of particle positions we relaxed the dipoles associated with the oxygens in a self-consistent iterative manner. This involved the calculation of the magnitude and direction of the electrical field at the location of each oxygen, and the gradual adjustment of the charge polarization in a direction that minimizes the total electrostatic energy of the system. Typically, three to eight iterations of this kind where necessary until the system's electrostatic energy changed by less than 1%.

Due to the Coulomb part, the particle interactions have a long range effect, which has certain implications on the computational procedure: In order to avoid surface effects, periodic boundary conditions are assumed. The ensemble is thought to be periodically replicated in three dimensions, that is, particles near a surface not only interact with their neighbor inside the simulation box but also with virtual images of particles from the opposite side of the box. This construct of periodic boundary conditions allows one furthermore to apply a numerical procedure, introduced by Ewald,[29,30] which causes the lattice summation of the long range Coulomb energies to converge more efficiently. The Ewald summation method consists in restructuring the expression for potential function such that part of it can be represented in reciprocal space and part in real space. This produces a potential which in real space has a reduced effective range. It can always be chosen such that the potential function decays to zero at the surface of the simulation box. The reciprocal space part of the force and energy summations can be done quite efficiently using fast Fourier transform algorithms.

This centrosymmetric potential function allows one to simulate the idealized structure of β cristobalite, which has the symmetry of the space group $Fd3m$. However, in this structure the Si–O distance is always equal to half of the Si–Si distance, which is in disagreement with the experiment. Therefore, a widely accepted model for the β cristobalite is one where the Si–O–Si bond angles are 147° instead of 180°, thus reducing the symmetry of this structure to that of the space group $Fdd2$. The deviation of the Si–O–Si bond from a straight line requires the introduction of an orientational term in the potential function ϕ_{ijk}, i.e., a term where the potential energy of a particle i depends on its position relative to the axis formed by two other particles j and k.

Various forms of three-body potentials have been conceived, and have been applied towards the simulation of different materials ranging from crystalline semiconductors to chalcogenite glasses.[6–9] We have tested two of the pub-

TABLE I. Potential parameters used for the simulation of the various silica structures. In case there are more than one number per field, the first one refers to the idealized cristobalite, the second to α and β cristobalite, and the third to amorphous silica.

Element	Charge	σ_i (nm)	n_i
Si	2.5 2.3 2.2	0.055 0.098 0.098	8
O	−1.25 −1.15 −1.1	0.147	8

Pair	A_{ij} (10^{-19} J)	C_{ij} (10^{-19} J)	ρ_{ij} (nm^{-1})	ζ_{ij} (nm)	η_{ij} (nm^{-1})
Si–Si	0.16	0.0	34.5	0.0	0.0
Si–O	0.56 0.22 0.22	25.56 8.434 8.38	42.4 36.0 36.0	0.7599 2.115 2.115	1.074
O–O	0.95	0.0	9.483	0.0	0.0

Triplet	γ_{ijk} (rad^{-2})	θ (rad)
Si–O–Si	0.0	3.14
	2.0	2.56
	0.9	2.56

lished potential forms, but finally resorted in developing a new variation. Our three-body term has the form,

$$\phi_{ijk}=(\varphi_{ij}+\varphi_{ik})e^{\gamma_{ijk}(\bar{\theta}-\theta_{ijk})^2}, \tag{7}$$

where $\varphi_{ij} = -C_{ij}e^{(\zeta_{ij}-r_{ij})\eta_{ij}}$. Here again, C_{ij}, γ_{ijk}, ζ_{ij}, η_{ij}, and $\bar{\theta}$ are empirical constants, whereas θ is the angle formed by the vectors $\mathbf{r}_{ij}$ and $\mathbf{r}_{ik}$. The values used for the various parameters are summarized in Table I. The three-body potential acts only between nearest neighbors, and for the simulations reported here it was necessary to introduce three-body terms only for the Si–O–Si combinations. Based on Pauling's electronegativity scale one may expect the Si–O bond to be of about half covalent and half ionic character. Accordingly, the charges on silicon and oxygen are reduced to almost half of their fully ionized charges.

III. RESULTS AND DISCUSSION

A. Generation of structures

The aim of this study was to simulate silica structures with various degrees of disorder, ranging from idealized cristobalite, over α and β cristobalite, a disordered form of β cristobalite, to amorphous silica. Graphical representations of these structures are compared in Fig. 2. In the aforementioned sequence, the silica structures exhibit a decreasing degree of regularity, which is reflected either in the actual loss of translational symmetry, or in the overall higher energy and reduced stability of the structure. The increasing degree of disorder in the structure is reflected in an increasing complexity of the corresponding vibrational spectra. In the following we will describe the procedures used to generate these structures, and discuss the concept of progressive irregularity by comparing structural geometry, phase stability, and vibrational spectra of the different modifications.

The atomic coordinates of the crystalline modifications of silica have been taken from the literature.[31] Cristobalite is one of the most commonly occurring crystalline polymorphs of silica. It is of particular interest to us because of its pseudocubic (α) or cubic (β) primitive cell. Based on the high degree of isotropy and symmetry, we expect the closest similarities in terms of the bonding to occur in cristobalite and in amorphous SiO_2. This strongly determines the short range structural order as well as the dynamic behavior, as reflected in infrared spectra. The high temperature (β) modification of cristobalite was originally perceived to have the so-called Wyckoff *C*9 structure,[32] and display the symmetry of the $Fd3m$ space group. In order to comply with both, the Si–O the Si–Si distance determined from x-ray diffraction patterns, one can picture the oxygens somewhat displaced from the line connecting the two adjacent silicons, such that the combination Si–O–Si forms an angle of approximately 147°. Following Leadbetter *et al.*[33] the positions of the silicon atoms remain unchanged as compared to the $Fd3m$ structure. It follows then that there are six equivalent orientations for the plane containing the Si–O–Si bonds.[33,34]

Low cristobalite has a tetragonal pseudocubic structure, which belongs to the space group $P4_12_12$.[31] There is relatively little distortion between the structures of high and low cristobalite (see Fig. 2). The simulations of all crystalline structures were started using as initial configurations the ideal coordinates published in the literature.[31–34] First the potential parameters were adjusted based on the sole criterion of furnishing the correct density for each structure. This was done in an approximate fashion, by using a static structure and by monitoring the forces in the first and second coordination shells of each atom. Provided that the first moments of these forces were

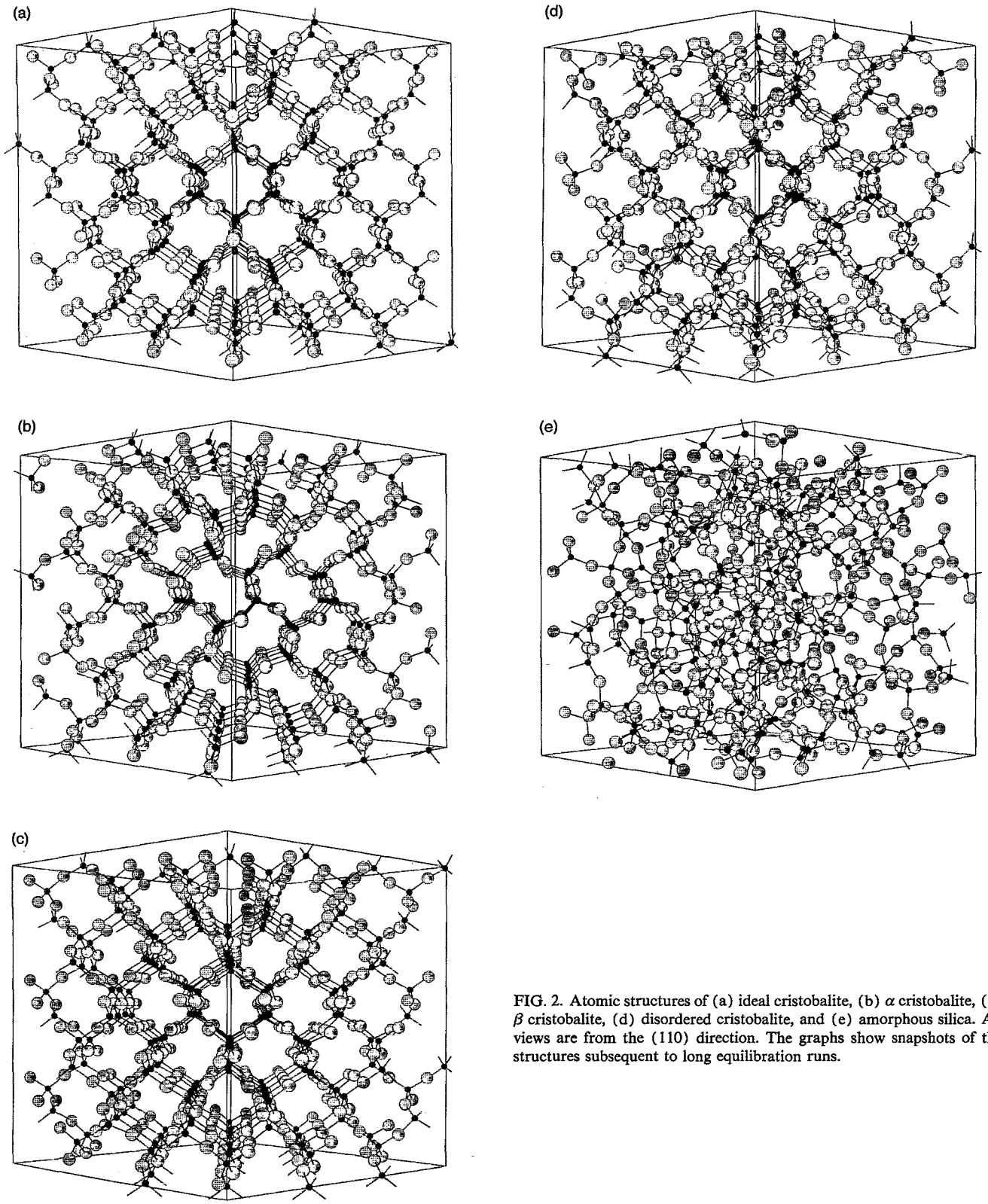

FIG. 2. Atomic structures of (a) ideal cristobalite, (b) α cristobalite, (c) β cristobalite, (d) disordered cristobalite, and (e) amorphous silica. All views are from the (110) direction. The graphs show snapshots of the structures subsequent to long equilibration runs.

approximately balanced, the structure was relaxed over several thousand iterations under constant pressure.

In case the structure remained stable, we then proceeded to record the time correlation functions of the dipole moments and calculated the complex dielectric response of the system. Initially, some minor adjustments with regard to the parameters that control the covalent part of the Si–O bond were necessary. The parameters were optimized to provide agreement between the frequencies of the simulated and experimentally observed Si–O stretching vibrations. The rest of the spectrum, i.e., the relative positions on the frequency axis of the other bands are predominantly a function of the structure. The general appearance of the spectrum cannot be changed significantly by chang-

ing the various potential parameters, without jeopardizing the stability of each crystalline structure. Furthermore, it was not possible to influence the vibrational frequency of the mode attributed to, say the Si–O stretch, by changing only those potential parameters that control this particular bond, without seeing an effect on the frequencies of virtually all other bands. This is, of course, a consequence of the complete connectivity of the structure in three dimensions, and it reflects the mechanism by which elastic waves propagate in solid. This strong correlation between the various spectral lines qualify the infrared spectrum as a unique characteristic of a given structure.

The phase transformation between α and β cristobalite occurs spontaneously and reversibly, based on a change of molar volume. It can be invoked either by thermal expansion or by imposing a tensile (α to β) or compressive (β to α) stress. Both modifications can be modeled with the exact same set of parameters, suggesting that there is not much change in the electronic structure, when going from one modification to the other.

Ideal cristobalite, on the other hand, required an adjustment of the parameters. In particular, the Si–O–Si bond angle is assumed to be 180° at equilibrium. This results in a larger intensity of the repulsion between silicons and oxygens, when maintaining the same density as for β cristobalite. The increased repulsion can be compensated with an increased ionicity (i.e., charge localization at the centers of mass) of these species, which generates dominating attractive forces between oppositely charged nearest neighbors. Ideal cristobalite can be viewed to be distortion free and has the highest symmetry. It produces the simplest spectrum, with only two well defined absorption bands (see Fig. 3). This structure and the corresponding spectrum will serve as a reference for our analysis. When moving from ideal cristobalite to amorphous silica, we gradually increase the degree of distortion of the structure. This distortion is reflected in the appearance of more and more features in the vibrational spectra.

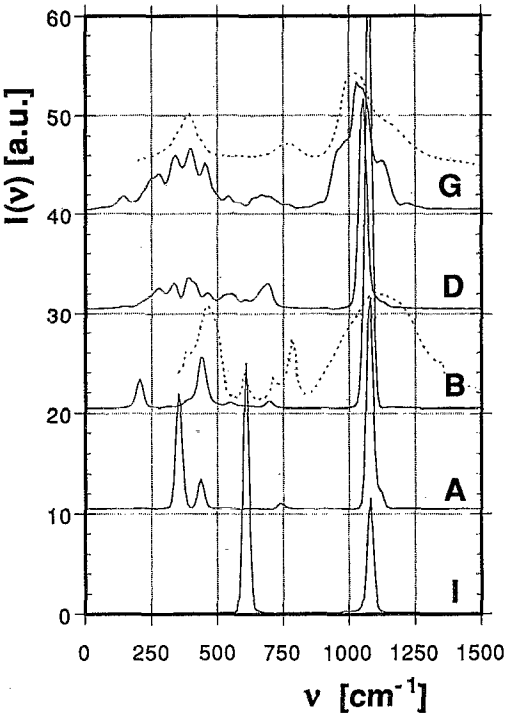

FIG. 3. Comparison of infrared absorption spectra of (I) ideal cristobalite, (A) α cristobalite, (B) β cristobalite, (D) disordered cristobalite, and (G) amorphous silica. (The baselines of the different spectra are offset by 10 units each, for the sake of clarity.) The experimental reflectance spectra for β cristobalite and silica glass are also shown as dashed lines.

B. Comparison of spectra

In Fig. 3 the spectra of the various simulated structures are compared, their baselines being offset for clarity. The experimental reflectance spectra of cristobalite and silica glass, as reported in the literature,[35,36] are included as dashed lines. The irreducible representations for α and β cristobalite have been reported by Wong and Angell.[37] Accordingly, there may be as many as 33 normal modes that could be either Raman or infrared active. Measured infrared spectra, on the other hand, exhibit a smaller number of spectral features, which can be grouped into two major and one minor bands: The highest-frequency band, ν_4 (nomenclature for the band frequencies chosen following that in Ref. 40) occurs at about 1070 wave numbers and is attributed to the Si–O asymmetric stretching modes. This is the band with the strongest intensity. The weakest band, ν_3, occurs at about 740 cm^{-1}. It is due to asymmetric deformations of the SiO_4 tetrahedra, which involve the motion of silicons as well as oxygens. The low-frequency band, ν_0, occurring at roughly 420 cm^{-1}, is caused by displacements of oxygens perpendicular to the direction connecting its neighboring silicon atoms, thus giving rise to a symmetric rocking motion of two neighboring SiO_4 tetrahedra about this connecting oxygen.[38–40] These bands are typically observed in amorphous silica as broad peaks.[40] Similar spectra have been reported for cristobalite, except that each band exhibits more features and may be split into several peaks, one occurring at 800 cm^{-1} and one at 630 cm^{-1}. The experimental spectrum for cristobalite is reproduced for comparison sake in Fig. 3. (The reader should bear in mind that the displayed spectrum has been determined in reflectance, which for adequate comparison with the simulated spectra would need to be converted according to the Kramers–Kronig formalism. This treatment usually reduces the widths of the observed spectral lines quite significantly.)

The spectrum of simulated ideal cristobalite, corresponding to the $Fd3m$ structure, is shown in Fig. 3 (I): it exhibits only two bands. Due to the high symmetry the low- and intermediate-frequency modes are degenerate and occur at the same frequency. This superposition of modes is also reflected in the high intensity of this band.

According to our results the low-frequency band of α-cristobalite splits into three peaks: one weak peak at 745 cm^{-1} and two stronger peaks occur at 350 and 440 cm^{-1}. This is in good agreement with experimental spectra. The transformation from α to β cristobalite solely affects the low-frequency doublet. It causes further splitting of the

low-frequency bands, in that the 350 cm^{-1} peak is shifted to 210 cm^{-1}, while the frequency of the 440 cm^{-1} peak remains unchanged. This peak is very characteristic of the structure. There is also a slight decrease in the frequency of the ν_3 peak.

In experimental spectra the various features of the low-frequency region are often merged into a broader band (see Fig. 3). This may in part be attributed to the instrument resolution. More likely though, it is the presence of defects, such as vacancies, impurities, dislocations, and grain boundaries, which causes this broadening. Note that the spectra shown in Fig. 3 are obtained from the simulation of perfect single crystals. The effect of deviations from an ideal crystalline structure can be seen in Fig. 3 (D), where the spectrum of disordered cristobalite is shown. The struture of disordered cristobalite was generated starting with a relaxed configuration of ideal cristobalite. When changing the ionic charges and equilibrium bond angles to those of real cristobalite, the structure relaxes to what one might describe as a disordered β cristobalite. The structure is fairly close to that of β cristobalite, except that the orientations of the planes containing the Si–O–Si triangles are random. In addition, this observation confirms the conclusion drawn from x-ray powder diffraction studies of Leadbetter *et al.*, which states that β cristobalite is made up of six equivalent groups of sixteen positions for the oxygen atoms, while the observed disorder may arise from a sixfold twinning mechanism.[33] As compared to the equilibrium β cristobalite, the spectrum of distorted cristobalite exhibits a much broader low-frequency band.

The next increment in structural disorder is attained with amorphous silica. The amorphous structure was generated by starting from random atomic coordinates. The starting configuration was stabilized at a temperature of 6000 K to allow for the preferred coordinations and the equilibrium density at this temperature to be reached. The configuration was then cooled to 800 K over 40 000 iterations (40 ps). The cooling was achieved by repeatedly rescaling the velocities of a small fraction of particles. The particles were selected at random; typically about 1–2 % of the total number of particles were subjected to this treatment at each time step. The new velocities assigned to these particles had random orientations and magnitudes that follow a Boltzmann distribution corresponding to the target temperature. Using this procedure, energy is removed more gently from the high temperature configuration. The chances of constraining the structure into a local energy minimum are reduced in comparison to the method where the velocities of all particles are rescaled simultaneously.

The spectrum of this simulated glass is shown in Fig. 3 (G). In comparison to those of the crystalline structures the absorption bands are much broader in case of the glass. The high-frequency peak shows shoulders, which are indicative for the existence of different coordination environments and, consequently, different bonding conditions for the bridging oxygens. Often the splitting of the high-frequency peak is attributed to the existence of dangling oxygens.[36] In our simulated structure all oxygens were coordinated by two silicons. In order to achieve this level of

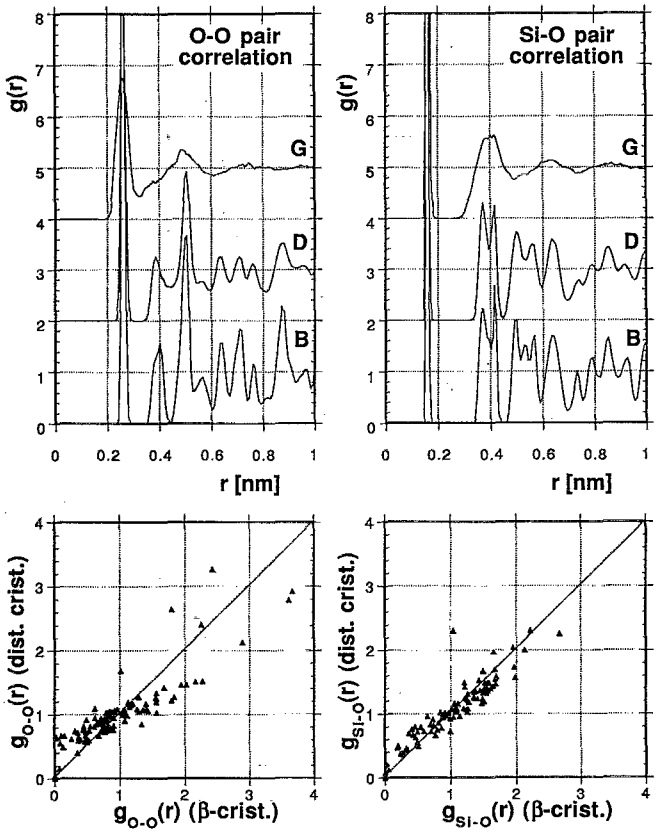

FIG. 4. Oxygen–oxygen and silicon–silicon pair correlation functions of β cristobalite (B), disordered cristobalite (D), and amorphous silica (G). The lower portions of the diagrams show the degree of correlation between the O–O and Si–O pair correlation functions of β and the disordered cristobalites.

completion in terms of coordination requirements, a large number of tetrahedral building blocks as well as Si–O–Si bond angles are distorted. As a result of these distortions, a spread of spring constants can be attributed to the positioning of oxygens with various degrees of alignment in Si–O–Si configurations; a condition which is sufficient to cause broadening and the formation of shoulders in the high-frequency peak of the infrared spectrum.

The low-frequency bands have an appearance rather similar to those of disordered cristobalite. As has been reported by several authors,[37,38] and as shown later, these modes can be attributed to vibrations of oxygen perpendicular to the line connecting its two neighboring silicons. With this in mind it is then interesting to compare the structural changes that occur when going from β cristobalite to distorted cristobalite to amorphous silica. In Fig. 4 the Si–O and O–O pair correlation functions of these three structures are plotted. One notices that the structural disorder introduced between β and distorted cristobalite affects mainly the coordination of oxygens by other oxygens, while the coordination of silicons by oxygens remains virtually unchanged. Consequently, the force field around the oxygens in directions perpendicular to the Si–Si axis varies from oxygen to oxygen. The resulting broadening in the range of force constants causes the splitting of the low-

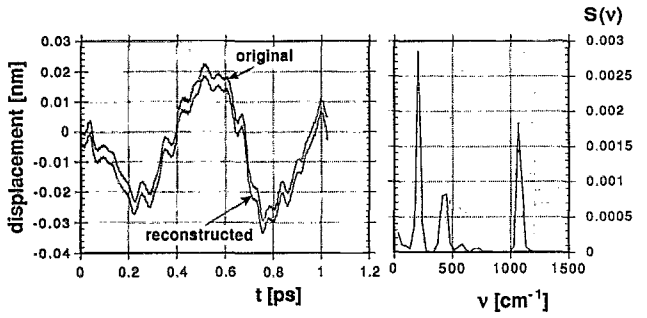

FIG. 5. Illustration of the Fourier transform filtering procedure for the identification of vibrational modes corresponding to the individual absorption bands in an infrared spectrum: simulated trajectory of a silicon atom (left diagram, upper curve); corresponding power spectrum obtained by Fourier transform (right diagram); reconstructed trajectory after a second Fourier transform (left diagram, lower curve).

frequency bands in the spectra of disordered cristobalite as well as of amorphous silica.

One important quest during spectral analysis is the assignment of atomic motions to the various bands in the spectrum. Using computer simulations of the dynamics of a structure, it is possible to simply "observe" the vibrational modes via a numerical model. In the course of such a simulation one can record the atomic positions as a function of time, yielding their trajectories. These trajectories are a composite of each vibrational mode, weighed by their respective amplitudes. In order to isolate those components of the atomic motion which are reflected in a specific spectral band, we used the following procedure. We start with the trajectory of particular atom, i.e., its x, y, and z coordinates as a function of time. First, each coordinate trace is Fourier transformed to yield the corresponding spectra. These spectra are somewhat different in nature than the infrared spectra. They usually contain more peaks, reflecting the entire motion of this atom, and not just those components which, in combination with the motion of oppositely charged particles yield a fluctuating dipole. Next, the spectral range corresponding to a certain infrared band is filtered out, by setting the spectral intensities outside of this range to zero. The filtered spectrum is then transformed back into a time domain signal, which corresponds to the component of the particles motion that is responsible for the selected infrared mode.

This procedure is summarized for β cristobalite in Fig. 5. In Fig. 5(a), the trajectory of a single oxygen particles is shown (solid line). The time interval is chosen such that the particle has returned to approximately its starting position. There is a slight discrepancy, reflecting the fact that the equilibrium position of this oxygen has drifted by a minute amount over the duration of a picosecond. The Fourier transform of this trajectory yields a complex spectrum, as shown in Fig. 5(b), and the inverse transform of the entire spectrum yields the lower line in Fig. 5(a). Note that this signal has been corrected for the drift, a property inherent to the Fourier transform. In Fig. 6 we show those components of the trajectory of this same oxygen, that contribute to the infrared bands at 440, 745, and 1070

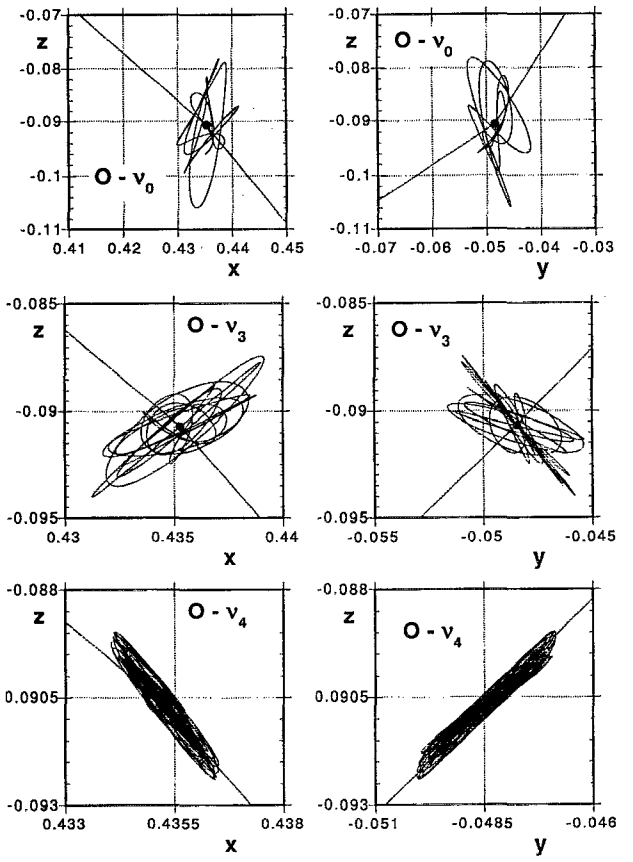

FIG. 6. Filtered trajectories of an oxygen particle responsible for the ν_0, ν_3, and ν_4 modes, respectively. Projections on the x-z and y-z planes are shown.

cm^{-1}, respectively. The projections onto the y-z and x-z planes are shown for clarity. To elucidate the orientations of these trajectories with respect to the positions of the neighboring silicons, the Si–O–Si bonds are represented by lines.

As one might expect, the higher the frequency, the smaller the amplitude of a vibration. The high-frequency mode is easily recognized as predominantly parallel to the Si–Si direction and, hence, corresponds to an asymmetric stretch. The trajectory producing the low-frequency mode is more complicated. It appears that the principal axis of the displacement is perpendicular to the Si–Si axis. A detailed analysis, however, reveals that only a modest excess amount of time is spent by the particle in this direction during its motion. The intermediate frequency mode can be attributed to a trajectory which has two principal axes, both forming an angle of about 67° with respect to the Si–Si axis, and they are symmetric with respect to the plane perpendicular to this axis (see Fig. 7).

IV. SUMMARY

An improved potential function has been developed, which allows for the modeling of various cubic modifications of SiO_2, including the dynamic simulation of the phase transformations between these modifications. Furthermore, this potential permits the simulation of infrared

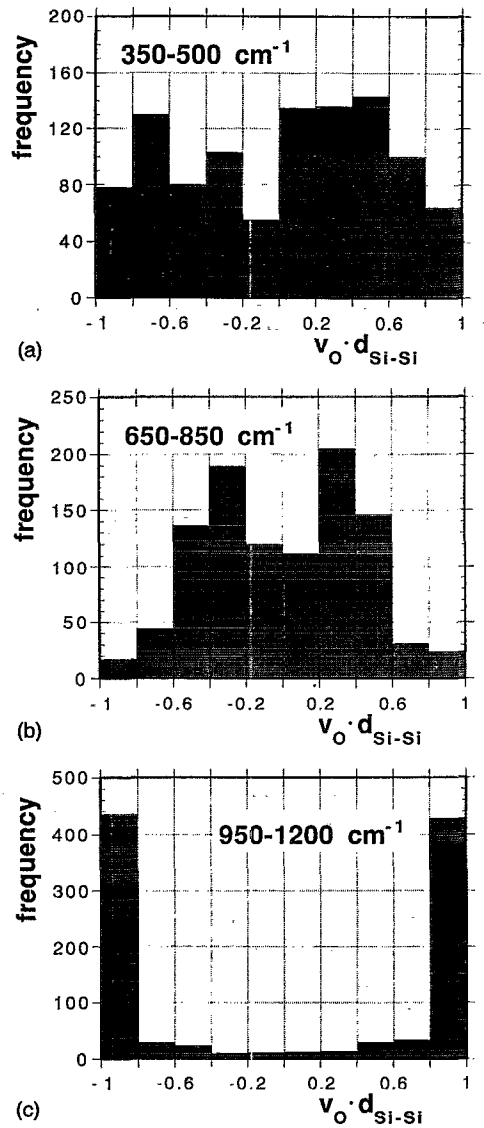

FIG. 7. Histograms showing the relative amounts of time spend by an oxygen atom in displacement, as a function of cosine of the angle that its trajectory forms with the line connecting its two neighboring silicons. The values are obtained by forming the scalar product of the unit vector in direction of the oxygen displacement with the unit vector describing the direction between its two neighboring silicons. The different distributions shown correspond to the (a) ν_0, (b) ν_3, and (c) ν_4 modes, respectively.

vibrational spectra that are in good agreement with the experiment. The simulation of a sequence of structures, ranging from that of ideal cristobalite to that of glass, was conducted to examine the effects of a progressive introduction of irregularity in the structures on the corresponding spectra. The analysis of pair correlation functions shows that a fair amount of disorder can be created between second nearest neighbors, especially in the oxygen sublattice, while the immediate coordination of silicon by oxygen remains undisturbed. The comparison of the structures and the corresponding spectra reveals that disorder in the oxygen sublattice influences predominantly the low-frequency bands.

The employment of a dynamic simulation technique allows one to perform a detailed analysis of the particle trajectories. In particular, a procedure has been developed which consists in Fourier transform filtering of particle trajectories, and permits one to identify those components of the particle's motion that are responsible for the different infrared absorption bands. This technique can be used to assist the interpretation of experimental spectra and the assignment of spectral bands to vibrational modes.

ACKNOWLEDGMENTS

This work was supported through a grant by Saint-Gobain Recherche, Paris, France and by the Pittsburgh Supercomputer Center under DMR900009P.

[1] M. P. Allen and D. J. Tildesley, *Computer Simulations of Liquids* (Oxford Science Publications, London, 1987).
[2] D. Fincham and D. M. Heyes, Adv. Chem. Phys. **63**, 493 (1985).
[3] L. V. Woodcock, C. A. Angell, and P. A. Cheeseman, J. Chem. Phys. **65**, 1565 (1976).
[4] A. Rahman, Phys. Rev. A **11**, 2191 (1975).
[5] T. F. Soules, J. Chem. Phys. **71**, 4570 (1979).
[6] F. H. Stillinger and T. A. Weber, Phys. Rev. B **31**, 5262 (1985).
[7] J. Tersoff, Phys. Rev. B **37**, 6991 (1988).
[8] P. Vashishta, R. K. Kalia, J. P. Rino, and I. Ebbsjö, Phys. Rev. B **41**, 12197 (1990).
[9] S. H. Garofalini, J. Chem. Phys. **76**, 3189 (1986).
[10] J. B. MacChesney and D. J. DiGiovanni, J. Am. Ceram. Soc. **73**, 3537 (1990).
[11] A. H. Narten, J. Chem. Phys. **56**, 1905 (1972).
[12] P. H. Gaskell, Phys. Chem. Glasses **8**, 69 (1967).
[13] J. B. Bates, J. Chem. Phys. **57**, 4042 (1972).
[14] A. J. Bennett and L. M. Roth, J. Phys. Chem. Solids **32**, 1235 (1971).
[15] A. G. Revesz, J. Non-Cryst. Solids **4**, 347 (1970).
[16] W. Wadia and L. S. Balloomal, Phys. Chem. Glasses **9**, 115 (1968).
[17] G. Lucovsky and R. M. Martin, J. Non-Cryst. Solids **8-10**, 185 (1972).
[18] R. J. Bell and P. Dean, in *Localized Excitations in Solids*, edited by R. F. Wallis (Plenum, New York, 1968), p. 124.
[19] P. N. Sen and M. F. Thorpe, Phys. Rev. B **15**, 4030 (1977).
[20] R. B. Laughlin and J. D. Joannopoulos, Phys. Rev. B **16**, 2942 (1977).
[21] A. Rahman and F. H. Stillinger, J. Chem. Phys. **55**, 3336 (1971).
[22] I. R. McDonald and L. V. Woodkock, J. Phys. C **3**, 722 (1970).
[23] J. Kieffer and C. A. Angell, J. Chem. Phys. **90**, 4982 (1989).
[24] R. Syed, J. Kieffer and C. A. Angell, Symp. Mat. Res. Soc. **135**, 73 (1989).
[25] D. A. McQuarrie, *Statistical Mechanics* (Harper and Row, New York, 1976).
[26] C. A. Angell, B. Boulard, J. Kieffer, and C. C. Phifer J. Non-Cryst. Solids **140**, 350 (1991).
[27] S. Brawer, J. Chem. Phys. **79**, 4539 (1983).
[28] M. L. Huggins and J. E. Mayer, J. Chem. Phys. **1**, 643 (1933).
[29] C. Kittel, *Introduction to Solid State Physics*, 6th Ed. (Wiley, New York, 1986).
[30] P. P. Ewald, Ann. Phys. **64**, 253 (1929).
[31] R. W. G. Wyckoff, *Crystal Structures*, 2nd Ed. (Interscience, New York, 1963).
[32] R. W. G. Wyckoff, Am. J. Sci. **9**, 448 (1925).
[33] A. J. Leadbetter, T. W. Smith, and A. F. Wright, Nat. Phys. Science **244**, 127 (1973).
[34] T. R Welberry, G. L Hua, and R. L. Withers, J. Appl. Cryst. **22**, 87 (1989).
[35] R. A. Nyquist and R. O. Kogel, *Infrared Spectra of Inorganic Compounds* (Academic, New York, 1971).
[36] J. Wong and C. A. Angell, in *Glass Structure by Spectroscopy* (Marcel Dekker, New York, 1976).
[37] J. Wong and C. A. Angell, Appl. Spectry. Rev. **4**, 155 (1971).
[38] F. L. Galeener, Phys. Rev. B **8**, 4292 (1979).
[39] F. L. Galeener, G. Lucovsky, and R. H. Geils, Phys. Rev. B **8**, 4251 (1979).
[40] F. L. Galeener, A. J. Leadbetter, and M. W. Springfellow, Phys. Rev. B **27**, 1052 (1983).